Front. Med. 2025, 19(6): 1099−1116
https://doi.org/10.1007/s11684-025-1166-y

RESEARCH ARTICLE

CYP4F11 promotes lung cancer progression through the miR-195/*ME2* pathway

Shan Shi[1,*], Jiao Zhou[2,*], Qiuyun Luo[3,*], Hongtao Chen[4,*], Jing Yang[1], Liqiong Yang[1], Lin Zhang (✉)[1], Hongyu Zhang (✉)[5], Dajun Yang (✉)[1]

[1]State Key Laboratory of Oncology in South China, Guangdong Provincial Clinical Research Center for Cancer, Sun Yat-sen University Cancer Center, Guangzhou 510060, China; [2]Cancer Center, the 10th Affiliated Hospital of Southern Medical University (Dongguan People's Hospital), Southern Medical University, Guangzhou 510280, China; [3]The First Affiliated Hospital (Shenzhen People's Hospital), Southern University of Science and Technology, Shenzhen 518055, China; [4]Department of Clinical Laboratory, The Fifth Affiliated Hospital of Sun Yat-sen University, Zhuhai 519000, China; [5]Department of Oncology, The Fifth Affiliated Hospital of Sun Yat-sen University, Zhuhai 519000, China

Abstract **The cytochrome P450 enzyme CYP4F11, a pivotal regulator of fatty acid metabolism and drug metabolism, exhibits significantly overexpression in non-small cell lung cancer (NSCLC) and is associated with poor clinical outcomes. Through integrated analysis of TCGA/GEO datasets and immunohistochemistry validation of 235 NSCLC specimens, we established *CYP4F11* as a novel prognostic biomarker. Functional studies demonstrated that *CYP4F11* knockdown markedly impaired NSCLC cell proliferation, clonogenicity, and migration *in vitro*, moreover xenograft models confirmed its tumor-promoting role *in vivo*. Mechanistically, we identified *CYP4F11* as a direct target of tumor suppressor miR-195 via 3′-UTR binding, with miR-195-mediated suppression of *CYP4F11* leading to ubiquitin-proteasomal degradation of mitochondrial malic enzyme 2 (ME2) — a critical metabolic regulator in cancer cells. Metabolomic analyses revealed that *CYP4F11* depletion disrupts mitochondrial malate metabolism, while rescue experiments confirmed *ME2*'s pivotal role in mediating *CYP4F11*'s oncogenic effects. Our findings elucidate the *CYP4F11*/miR-195/*ME2* regulatory axis as a crucial determinant of NSCLC progression, highlighting *CYP4F11* as both a prognostic indicator and a potential therapeutic target through modulation of cancer cell metabolism.**

Keywords CYP4F11; miR-195; ME2; ubiquitination degradation

Introduction

The latest data from 2025 shows that lung cancer is still the cancer with the highest incidence and mortality rate in China and even in the world [1]. Among the delineated lung cancer subtypes, non-small cell lung cancer (NSCLC) is preeminent, constituting ~85% of cases [2]. Owing to its aggressive phenotype, NSCLC exacts a profound impact on patients [3]. It is indispensable to identify the key molecule as a treatment target and develop novel effective targeted therapies to improve patient prognosis.

The human cytochrome P450 (CYP) superfamily consists of 57 genes [4]. The enzymes encoded by these genes can play a role in the synthesis and metabolism of steroids, metabolism of xenobiotics, drugs, arachidonic acid, and eicosane compounds, hydroxylation of retinoic acid, cholesterol metabolism and biosynthesis of cholic acid. The human cytochrome P450 4F (CYP4F) gene subfamily is composed of 7 different enzymes, including *CYP4F2*, *CYP4F3a*, *CYP4F3b*, *CYP4F8*, *CYP4F11*, *CYP4F12*, and *CYP4F22*, with 74% homology in their amino acid sequences. *CYP4F2*, *CYP4F3b*, *CYP4F11*, and *CYP4F12* are expressed in the liver and kidneys [5–7], while *CYP4F3a* is only expressed in the medullary tissue [8], and *CYP4F8* is only expressed in the seminal vesicles [9].

CYP4F11 was found by Xiaoming Cui *et al*. through library search and cDNAs rapid amplification analysis to

Received April 1, 2025; accepted August 4, 2025

Correspondence: Dajun Yang, yangdj@sysucc.org.cn;
Hongyu Zhang, zhhyu@mail.sysu.edu.cn;
Lin Zhang, zhanglin@sysucc.org.cn

*These authors contributed equally to this work and should be considered co-first authors.

contain 1765 nucleotides, encoding 524 amino acids [10]. Compared with *CYP4F2*, *CYP4F3*, and *CYP4F8*, *CYP4F11* was 80.0%, 82.3%, and 79.2%, respectively [11]. The molecular weight of CYP4F11 is approximately 57 kDa, which is consistent with the late-stage molecular weight of calcium. It is mainly expressed in the human liver, followed by the kidneys, heart, and skeletal muscles [12]. However, CYP4F11 is still considered an "orphan" enzyme, as its function has not been fully described [13]. Some studies have explored the catalytic activity of CYP4F11 expressed in brewing yeast, with certain drugs (such as erythromycin) exhibiting higher oxidation rates and some endogenous eicosane compounds (such as leukotriene B4) exhibiting lower oxidation rates [14]. In addition, it has been reported that sensitive cell lines expressing CYP4F11 can metabolize these compounds into irreversible stearyl-CoA desaturase (SCD) inhibitors. SCD is considered a promising biological target for the treatment of cancer and metabolic diseases [15]. Therefore, it provides a strategy to target SCD in tumors by using highly expressed CYPs in tumor subgroups, to achieve the effect of inhibiting tumor progression [16]. Strongly suggesting that *CYP4F11* may affect cancer progression by affecting compound metabolism, this study was conducted to further investigate its role in lung cancer.

Our research group previously identified *CYP4F11* as a gene highly expressed in patient-derived xenograft (PDX) tissues with metastasis (compared to PDX tissues without metastasis) through transcriptome sequencing, which is approximately 3.6 times higher, providing us with important clues. By analyzing data from lung cancer patients in The Cancer Genome Atlas (TCGA) and Gene Expression Omnibus (GEO) databases, we also found that *CYP4F11* is generally highly expressed in lung cancer patients and is associated with poor prognosis, especially in NSCLC. These findings suggest that *CYP4F11* may be a potential biomarker and therapeutic target for NSCLC.

Here in this study, we intend to explore the functions and potential mechanisms of *CYP4F11* in NSCLC. We observed that *CYP4F11* is highly expressed in NSCLC and positively correlated with poor overall survival. Reducing the expression of *CYP4F11* subsequently inhibited its promoting function of migration, clonogenicity, and cell proliferation. We also found that miR-195 binds to the *CYP4F11* promoter region, with *CYP4F11* being a downstream target of miR-195. Furthermore, we reported that *CYP4F11* localizes to the mitochondria, and the frequent low expression of *CYP4F11* in NSCLC resulted in ubiquitination degradation of ME2 which inhibited the progression of NSCLC. ME2 is a mitochondrial metabolic enzyme that catalyzes the oxidation and decarboxylation of malic acid to produce pyruvic acid, accompanied by the production of NADPH. It plays an important role in the progression of various cancers. Our study uncovers *CYP4F11* as an important regulator of NSCLC growth and metastasis and holds the promise to provide effective treatment strategies for NSCLC.

Materials and methods

Lung cancer tissue samples

Fresh frozen paired samples of lung cancer tissues and adjacent normal tissues were obtained from the Oncology Department of The Fifth Affiliated Hospital of Sun Yat-sen University. All human sample research was reviewed and approved by the Ethics Committee of Sun Yat-sen University Cancer Center (No. K112-1), and patients informed written consent was obtained from all donors.

Immunohistochemistry

A total of 240 lung adenocarcinoma tissue samples from lung adenocarcinoma patients were chosen for immunohistochemistry randomly, which were embedded in paraffin and sectioned. Sections (4 μm thick) were deparaffinized and rehydrated with PBS (pH 7.4). Samples were blocked with 5% (m/v) bovine serum albumin (BSA) for 30 min at room temperature, then the rabbit anti-CYP4F11 monoclonal antibody (No. PA5-113387, Thermo Fisher Scientific, USA) was diluted 1:100 in 1% BSA and incubated with the tissue sections at 4 °C overnight. Next, they were incubated with a secondary antibody conjugated with diaminobenzidine (DAB) at room temperature for 15 min and then washed with PBS. Finally, the cell nucleus was dyed with Harri's hematoxylin solution.

Cell culture

The human normal bronchial epithelial cell line (BEAS-2B) and lung cancer cell lines (PC9, H292, H1650, A549, H1993 and H226 cells) were obtained from The Cell Bank of Type Culture Collection of The Chinese Academy of Sciences. All cells were cultured in DMEM supplemented with 10% fetal bovine serum (FBS, Thermo Fisher Scientific, USA) and antibiotics (100 U/mL penicillin-streptomycin) in a humidified atmosphere containing 95% air and 5% CO_2 at 37 °C.

Transfection with siRNA

A549 and PC9 cells were used for the knockdown of *CYP4F11* by siRNA transfection. Cells were seeded in 60 mm tissue culture dishes (35 000 cells per dish) overnight. Transfection of *CYP4F11* siRNA (Ribobio, Guangzhou, China) was performed using Lipofectamine RNAiMAX (Invitrogen, Thermo Fisher Scientific, USA)

according to the manufacturer's protocol. At 24–48 h after transfection, cells were collected for RNA and protein expression to confirm knockdown and plated for cell proliferation experiments.

Stable transduction with single-guide RNA (sgRNA) targeted to *CYP4F11*

The knockout fragment targeting *CYP4F11* was stably transfected into cells by the lentivirus method. HEK-293T cells were cultured in a 6-well plate with a complete culture medium the day before and transfected when the cell confluence was about 90%. Using a plasmid lentiviral packaging system, two packaging plasmids psPAX2, PMD2.G (Thermo Fisher Scientific, USA), and the target gene were mixed in the amount of 3 μg: 2 μg: 1 μg, respectively. Then polyethylenimine (PEI) was added in the amount of a quarter of plasmid. Finally, 200 μL Opti-MEM medium was added to the mixture, which was gently pipetted and added dropwise to the cells. After 6–8 h, the solution was changed to a complete medium. After 48 h, the cell culture supernatant was collected and filtered with a 0.22 μm filter membrane to obtain the virus solution. The green fluorescent protein was observed by fluorescence microscope to determine whether the transfection was successful. Stably transduced cell lines were established using puromycin selection. We screened three short hairpin sgRNAs targeting human *CYP4F11* transcripts and found one independent sequence that decreased mRNA levels by more than 70%. The sgRNA sequences are as follows:

CYP4F11-sgRNA (1): GGGGATATGTGGTCACCAGC;
CYP4F11-sgRNA (2): GTCTTCATGCCCTCTTCCGT;
CYP4F11-sgRNA (3): GTGATAGGCCGGATAATGTC.

Extraction of RNA and quantitative real-time reverse transcription polymerase chain reaction (qRT-PCR)

The TRIzol method was used to extract total RNA from cell lines, then transformed into cDNA using PrimeScript RT Master Mix (TAKARA, Guangzhou, China). The expression of 6 hub genes was measured by qRT-PCR using the commercial kit TB Green Premix Ex Taq II (Tli RNaseH Plus) (TAKARA, Guangzhou, China) and a LightCycler 480 II System 373 (Roche, USA). β-actin was used to normalize *CYP4F11* expression. The primers used were as follows:

CYP4F11 Forward: 5′-ACTCAGGGTATTGATGATTT-3′, and Reverse: 5′-AGGACCCAGGAGAGACCACT-3′.
β-actin Forward: 5′-TGACGTGGACATCCGCAAAG-3′, and Reverse: 5′-CTGGAAGGTGGACAGCGAGG-3′.

Western blot

Cell lysates were prepared using Cell Lysis Buffer (Cell Signaling Technology) according to the manufacturer's protocol. Protein concentrations in cell lysates were measured using the bicinchoninic acid (BCA) protein assay reagent (Pierce, Rockford, IL). Equal amounts of protein per sample were resolved on 10% sulfate-polyacrylamide gel electrophoresis (SDS-PAGE) under reducing conditions and then transferred to a nitrocellulose membrane. After being blocked with 5% BSA in tris-buffered saline (TBS) with 0.1% Tween 20, the membranes were incubated with different primary antibodies as indicated in figures overnight at 4 °C, washed three times with 0.1% Tween 20-TBS (TBST) and then incubated for 60 min with 1:4000 peroxidase-conjugated anti-rabbit IgG or anti-mouse IgG. The membrane-bound peroxidase activity was detected using ECL Prime Western Blot Detection kits (Amersham, Arlington Heights, IL). Image J 1.32j software (National Institute of Health, MD) was used to quantify band intensity.

Cell proliferation and growth assay

Cell viability was determined using Cell Counting Kit-8 (CCK-8, GOONIE) according to the manufacturer's instructions. Cells were pretreated with sgRNA-targeted *CYP4F11* or control sgRNA in 96-well plates at a density of 2000 cells per well. CCK-8 (10 μL) was added into 100 μL serum-free DMEM medium and incubated at 37 °C for 1 h. The optical density (OD) value was measured by a spectrophotometer reader (Thermo Fisher Scientific, USA) at an absorbance of 450 nm once per day for 4 d.

Colony formation assays

Two milliliters of culture medium containing 2000 cells were seeded in each well of 6-well plates. After 2 weeks of culture in an incubator at 37 °C with 5% CO_2, the cells were fixed in 4% (w/v) paraformaldehyde (Biosharp, China), then stained with a crystal violet solution (Merck, Germany) and photographed.

Migration assays

Lung cancer cell migration abilities were detected by the Transwell assay, using 24-well Boyden chambers (BD Inc., USA) with an 8-μm pore size. 2×10^5 PC9 cells and 1.5×10^5 A549 cells were seeded on each Transwell inserts and incubated in 200 μL of serum-free DMEM at 37 °C in the upper chambers for 42 h and 19 h, respectively; DMEM medium containing 10% FBS was added to the lower chamber. Cells that traversed the inserts to the underside chamber surface were fixed, stained, and observed under phase-contrast microscopy.

Xenograft lung cancer model

This study was approved by the Animal Ethical and Welfare Research Committee of Sun Yat-sen University and performed according to established guidelines. For the subcutaneous transplant xenograft model, female nude mice aged 4–5 weeks were used for the animal experiment. Stable *CYP4F11*#2 knockout A549/PC9 cells (5×10^6 per mouse) and a non-sense hairpin A549/PC9 cells (5×10^6 per mouse) were used and inoculated subcutaneously into left flanks of nude mice (7 mice per group). After 7 d, palpable tumors had developed. Tumor volumes were calculated based on tumor width (W) and length (L) ($W^2 \times L/2$, with $W < L$). Mice were euthanized when their tumors reached 1.5 cm in diameter.

Target microRNA prediction of *CYP4F11*

To predict the target genes of miR-195, we conducted a bioinformatics analysis using a panel of different algorithms including DIANAmT, Miranda, miRDB, PICTAR5, RNA22, TargetScan, and miRWalk.

Human miR-195 mimic (miR-195) and the corresponding negative control mimic (miR-NC) were purchased from GenePharma Co., Ltd. (Shanghai, China).

Luciferase reporter assay

The wild-type 3′-UTR segment and a mutant 3′-UTR segment of *CYP4F11* cDNA were amplified by PCR and then inserted into the luciferase gene using the psiCHECK-2 vector (Promega Corporation, Madison, WI, USA), according to the manufacturer's instructions. Luciferase assay was then performed in A549 and PC9 cells, during which tumor cells (1×10^5 cells per well) were seeded into 24-well plates and grown overnight. On the following day, 100 ng luciferase reporter vectors and 100 nmol/L miR-195 or miR-NC were transfected into the A549 and PC9 cells using Lipofectamine® 3000 (Invitrogen, Thermo Fisher Scientific, USA) for 48 h. Thereafter, the cell protein was extracted and the luciferase activity was measured using a luciferase reporter assay system (Promega Corporation), according to the manufacturer's protocol.

Immunofluorescence

Cells for immunofluorescence were seeded at the glass bottom cell culture dish and permeabilized with 0.2% (v/v) Triton X-100 in PBS for 20 min. After washing 3 times in PBS, cells were then blocked in PBS containing 3% BSA for 1 h at room temperature. The primary antibodies (Cell Signaling Technology) were diluted in the blocking buffer (1:200) and incubated at 4 °C overnight. Alexa Fluor conjugated secondary antibodies (Invitrogen) were diluted in PBS (1:1000) and incubated with cells at room temperature for 1 h. Thereafter, 4',6-diamidino-2-phenylindole (DAPI) (1:10 000) was used for counterstaining the nuclei.

Determination of mitochondrial DNA content

Mitochondrial DNA content was determined as described previously with modifications. Briefly, total genomic DNA was isolated using a DNeasy blood & Tissue Kit (Qiagen, Cat# 69504) according to the manufacturer's instructions. Mitochondrial DNA content was quantified using qRT-PCR using mitochondria-specific primers for (1) D loop: 5′-GATTTGGGTACCACCCAAGTATTG-3′ and 5′-GTACAATATTCATGGTGGCTGGCA-3′ and (2) Cytochrome b: 5′-TGAAACTTCGGCTCACTCCT-3′ and 5′-AGCTTTGGGTGCTAATGGTG-3′. 18S rDNA-specific primers (5′-TAGAGGGACAAGTGGCGTTC-3′ and 5′-CGCTGAGCCAGTCAGTGT-3′) were used to quantify nuclear DNA content and were used as an internal control for normalization.

Malic acid determination

The Malic Acid Colorimetric Assay Kit (Elabscience, Cat# E-BC-K905-M) was used to detect malic acid concentration in cells. Cells were collected for ultrasound homogenization, and centrifuged at 10 000 *g* for 10 min at 4 °C. 100–500 μL of supernatant were added to 10 kDa ultrafiltration tube, and centrifuged at 12 000 *g* for 15 min, and take the filtrate were taken from the outer tube for testing. Prepare a concentration gradient standard solution according to the operation steps of the reagent kit, add each reagent to a 96-well plate, and set three multiple wells for each sample. After incubation at 37 °C for half an hour, measure the OD value at 450 nm using a spectrophotometer reader (Thermo Fisher Scientific, USA), draw a standard curve, and calculate the malic acid content of different groups.

Co-immunoprecipitation (co-IP)

Cells were harvested and lysed with mild RIPA buffer directly on the plate for 15 min. Meanwhile, 25 μL DynaGreen™ Protein A/G beads (Thermo Fisher Scientific, USA) were incubated with 3 μg antibody at room temperature for 1h. Then mix the protein lysate with the beads-antibody complex and incubate overnight at 4 °C. Beads were washed three times with lysis buffer. Bound proteins and 10% inputs were detected by immunoblotting (IB).

***In vivo* ubiquitination assay**

A549 and PC9 cells were transfected with different

combinations of plasmids loading *si-CYP4F11*, *HA-ME2*, and *His-Ub*. After 48 h, cells were harvested and divided into two parts, one for IB and the other for the ubiquitination assay. Briefly, cell pellets were lysed with buffer I (8 mol urea, 0.1 mol Na_2HPO_4/NaH_2PO_4 (pH 8.0), 10 mmol/L Tris-HCl (pH 8.0), 10 mmol/L β-mercaptoethanol, 5 mmol/L imid-azole) and incubated with Anti-His Magnetic Beads (MCE, Shanghai) for 4 °C overnight. Beads were washed twice with TBST. The bound protein complex was eluted and analyzed by IB.

Statistical analysis

All data were obtained from two or three independent experiments and are presented as mean ± SD. We performed statistical analysis with GraphPad Prism (version 7.00), using the unpaired, two-tailed Student's *t*-test module, where "ns" represents no statistical significance, * represents P value < 0.05, ** represents P value < 0.01, *** represents P value < 0.001, and **** represents P value < 0.0001. Graphs were plotted with GraphPad Prism software as well. Kaplan-Meier survival analyses were used to compare survival among lung cancer patients based on *CYP4F11* expression. Western blot bands were quantified with Image-Pro Plus, and the results of target protein were normalized to GAPDH. Colocalization between two stained proteins was analyzed by ImageJ (version 1.53e). Representative immunofluorescence results were based on three independent experiments. Statistical significance was defined as $P < 0.05$.

Results

CYP4F11 is upregulated in lung cancer and correlates with poor survival

Our research group previously identified *CYP4F11* as a highly expressed gene in PDX tissues with metastasis (compared to PDX tissues without metastasis) through transcriptome sequencing, which is approximately 3.6 times higher (Fig. 1A). Further exploration from the Kaplan-Meier Plotter database showed that elevated *CYP4F11* expression was correlated with poor cancer survival (P = 0.00022, Fig. 1B). Moreover, we also used GEPIA to compare *CYP4F11* expression between normal tissue and NSCLC tissue and found that its expression in NSCLC was significantly higher ($P < 0.05$, Fig. 1C). To further demonstrate whether *CYP4F11* is widely expressed in normal tissues, we selected human normal tissue samples such as liver, kidney, spleen, calf, cervical lingual muscle, and medial pterygoid muscle for immunohistochemistry. The results showed that CYP4F11 is only highly expressed in liver and kidney tissues, while low or no expression is observed in other tissues (Fig. S1A). Then we conducted immunohistochemical staining on the cancerous tissue and its corresponding adjacent tissues of 235 NSCLC patients to evaluate their H-scores. Among them, 28 cases were excluded due to loss of follow-up. We found that *CYP4F11* is mainly localized in the cytoplasm and its expression of *CYP4F11* in the tumor tissues of lung cancer patients is significantly higher than in adjacent tissues (Fig. 1D). Kaplan-Meier survival analysis showed that the overall survival rate of patients with high *CYP4F11* expression (n = 103) was lower than that of patients with low *CYP4F11* expression (n = 104) (P = 0.0039, Fig. 1E). The mortality rate of patients with high expression of *CYP4F11* is higher than that of patients with low expression. The clinical and pathological characteristics of the patients included in this study are summarized in Table 1. The expression of *CYP4F11* is not associated with age, gender, smoking, TNM staging, and clinical staging. However, in patients with lower survival rates, the expression level of *CYP4F11* is relatively higher (**$P < 0.01$). Univariate Cox regression analysis showed that high expression of *CYP4F11* increased the risk of death compared to low expression of *CYP4F11* (hazard ratio (HR) 2.030, 95% CI 1.240–3.324, P = 0.005). Multivariate Cox regression analysis showed that *CYP4F11* expression was an independent predictor of poor survival in patients (HR 1.924, 95% CI 1.172–3.159, P = 0.010), as shown in Table 2.

Selecting human normal lung epithelial cells BEAS-2B and human lung cancer cell lines such as PC9, H292, H1650, A549, H1993, and H226 for qRT-PCR detection, it was found that the expression of *CYP4F11* in A549, H292, PC9 cells were higher than that in BEAS-2B cells, with the highest expression observed in A549 and PC9 cells. The expression of *CYP4F11* in H1993 cells is lower than that in BEAS-2B (Fig. 1F). Western blot detection results showed that compared with BEAS-2B cells, the protein levels of CYP4F11 in A549, H292, and PC9 cells were significantly increased (*$P < 0.05$, Fig. 1G). Among them, A549 and PC9 cells showed the highest protein expression levels. The expression of CYP4F11 in H1650 and H292 cells was lower than in BEAS-2B cells. Therefore, we selected A549 and PC9 cells for subsequent knockdown experiments.

Knockdown of *CYP4F11* by siRNA inhibits the growth of NSCLC cells *in vitro*

To further evaluate the effect of *CYP4F11* on the biological functions of NSCLC cells, we used siRNA to knock down *CYP4F11* expression in A549 and PC9 cells. Western blot showed that both siRNAs decreased the expression level of CYP4F11 in A549 and PC9 cells, but siRNA target sequence 2 (si2) was more efficient, reducing CYP4F11 expression by at least 80% (Fig. 2A

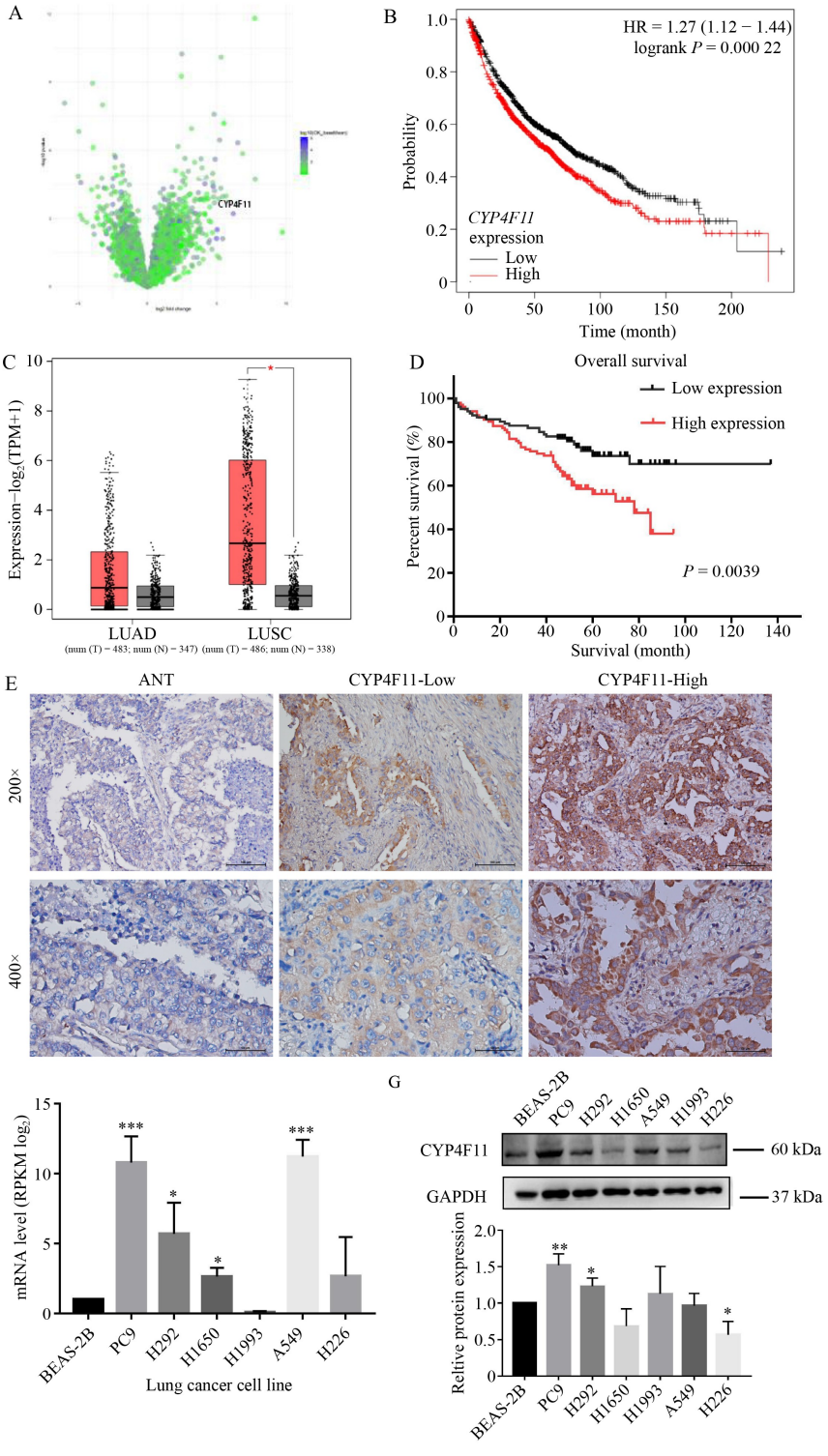

Fig. 1 *CYP4F11* is highly expressed in lung cancer, while its high expression is associated with poor patient outcomes. (A) The sequencing results of the PDX model constructed by our research group in the early stage indicate that *CYP4F11* is highly expressed in lung cancer patients with metastasis. (B) High *CYP4F11* expression is associated with shorter overall survival (OS) in lung cancer patients (***$P < 0.001$). (C) Compared with normal tissues, the expression level of *CYP4F11* in LUAD and LUSC samples was significantly increased. (D) Kaplan–Meier survival analysis indicated that higher protein expression of CYP4F11 was significantly associated with lower OS in NSCLC patients. The data were expressed as the mean ± S.D. **$P < 0.01$. (E) Pathological tissue includes adjacent normal tissue and lung cancer tissue. Representative IHC images of CYP4F11 expression in adjacent normal tissue (ANT), and images of low (LOW) and high (HIGH) CYP4F11 expression in NSCLC. The scale bars represent 50 μm. (F) Steady-state levels of *CYP4F11* mRNA in different human lung cancer cell lines as quantified using qRT-PCR. (G) CYP4F11 protein levels were determined by the Western blot analysis in various cell lines and paired normal lung epithelial cells.

Table 1 Statistical analysis of the correlations between *CYP4F11* expression and the clinicopathological parameters

Characteristics	*CYP4F11*		*P* value
	Low expression	High expression	
Age (year)			
⩾ 60	64	67	
< 60	40	36	0.60#
Gender			
Male	55	52	
Female	49	51	0.73#
Smoke			
No	74	74	
Yes	30	29	0.91#
T stage			
T1 + 2	93	91	
T3 + 4	11	12	0.80#
M stage			
M0	98	98	
M1	6	5	0.77#
N stage			
Negative	86	78	
Positive	18	25	0.21#
Clinical stage			
I + II	86	76	
III + IV	18	27	0.12#
Survival			
Alive	78	59	
Deceased	25	44	0.005**

$^{**}P < 0.01$, $^{\#}P > 0.05$.

and 2B). Therefore, we chose the *CYP4F11*-homo2 siRNA sequence to silence the *CYP4F11* gene in NSCLC cells in subsequent experiments. We observed that the knockdown of *CYP4F11* inhibited the migration of NSCLC cells via Transwell assays (Fig. 2C). Moreover, we performed plate colony formation and CCK-8 assays to detect cell growth in A549 and PC9 cell lines. The results showed that downregulation of *CYP4F11* significantly suppressed the proliferation of NSCLC cells (Fig. 2D and 2E). Thus, *CYP4F11* could promote the proliferation and migration of A549 and PC9 cell lines *in vitro*.

CYP4F11 knockout mediated by CRISPR-Cas9 inhibits cell proliferation and migration of A549 and PC9 cell lines

The knockout efficiency of *CYP4F11* mediated by CRISPR-Cas9 was analyzed in both protein and mRNA levels (Fig. 3A and 3B), and *CYP4F11*-sgRNA (2) showed the best inhibition effect. The colony formation assay and cell growth curve in A549 and PC9 cells were performed. A549 and PC9 cells treated with *CYP4F11*-sgRNA (1) and *CYP4F11*-sgRNA (2) significantly inhibited colony formation rate and cell growth compared with cells treated with NC-sgRNA (Fig. 3C and 3D). To evaluate the effect of *CYP4F11* on cell migration, we knocked out *CYP4F11* in A549 and PC9 cell lines using *CYP4F11*-sgRNA (1) and *CYP4F11*-sgRNA (2). The results of the Transwell assay suggested that migration was significantly inhibited in cells treated with both sgRNAs compared with the NC-sgRNA group (Fig. 3E).

Table 2 Univariate and Multivariate Cox regression analysis of multiple prognostic factors in lung cancer patients

	Univariate analysis			Multivariate analysis		
	P	HR	95% CI	*P*	HR	95% CI
CYP4F11	0.005	2.030	1.240–3.324	0.010	1.924	1.172–3.159

Stable knockout of *CYP4F11* reduces tumor growth in mouse xenograft models

To evaluate tumorigenesis *in vivo*, a tumor xenograft model was established following *in vitro* studies that confirmed the tumor-promoting effect of CYP4F11 in NSCLC. A549-sgNC and A549-*CYP4F11*-sgRNA (2), PC9-sgNC and PC9-*CYP4F11*-sgRNA (2) cells were separately injected subcutaneously into the flanks of nude mice to establish xenografts. Tumor sizes were measured twice a week and were significantly reduced in xenografts deriverd from A549-*CYP4F11*-sgRNA (2) and PC9-*CYP4F11*-sgRNA (2) (Fig. 4A). The mice were sacrificed after 4 weeks later, and the tumor xenografts were dissected and weighed. The results indicated a significant reduction in both tumor weight and tumor volume following knockout of *CYP4F11* ($^{**}P < 0.01$, Fig. 4B and 4C). Taken together, these *in vivo* experiments also indicated that *CYP4F11* knockout via CRISPR-Cas9 inhibited the growth of NSCLC cells.

CYP4F11 is the direct target of miR-195

Since miRNAs alter the expression of their target genes to exert their biological functions in cells, bioinformatic analysis was performed using several software (DIANAmT, miRanda, miRDB, miRWalk, PICTAR5, RNA22, and TargetScan) to predict the possible targets of miR-195 (Fig. S1B and S1C). Subsequently, relevant publications on these microRNAs were retrieved from PubMed, and microRNAs that have been widely studied in lung cancer and were not highly expressed in other tumors were excluded. The data revealed that the miR-195 mimic was successfully transfected into the cells and increased miR-195 expression, while miR-NC

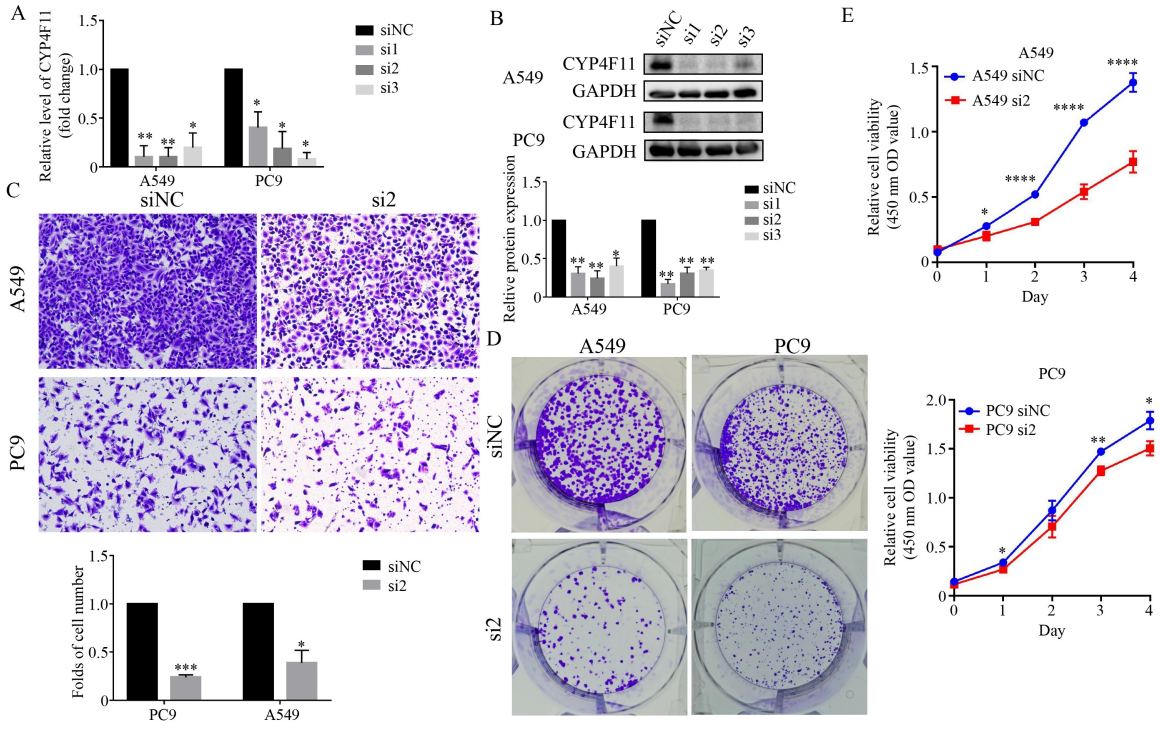

Fig. 2 siRNA-mediated knockdown of *CYP4F11* reduces the proliferation and metastasis ability of A549 and PC9 cells. (A) Knockdown efficiency of *CYP4F11* in A549 and PC9 cells by qRT-PCR analysis. (B) CYP4F11 protein expression in A549 and PC9 (high *CYP4F11* expressing human lung cancer cell line) transfected with non-targeting (NC) or *CYP4F11* siRNA. Transfection with *CYP4F11* siRNA decreased CYP4F11 protein expression. (C) A Transwell assay was performed to determine the motility of A549 and PC9 cells cotransfected with *CYP4F11* siRNA (magnification 200×). (D) Colony-forming and (E) Cell Counting Kit-8 (CCK-8) assays were used to detect the cell viability of A549 and PC9 cells cotransfected with *CYP4F11* siRNA.

transfection had no significant effect on the A549 and PC9 cells (Fig. 5A). Finally, it was detected that miR-195 bound to the 3′-UTR of *CYP4F11* cDNA. This binding ability of miR-195 to the *CYP4F*11 3′-UTR was then confirmed using a luciferase reporter assay. The results revealed that miR-195 was able to precisely bind to the wild-type 3′-UTR of *CYP4F11*, which resulted in significantly inhibited luciferase activity (Fig. 5B). Furthermore, it was demonstrated that miR-195 overexpression in A549 and PC9 cells significantly downregulated the mRNA (Fig. 5C) and protein (Fig. 5D) levels of CYP4F11.

The *in vitro* data further supported this observation. Overexpression of miR-195 significantly inhibited the transcription of *CYP4F11*, thereby reducing the proliferation (Fig. 5E) and migration (Fig. 5F). To further confirm that *CYP4F11* is the target of miR-195, we added *CYP4F11* overexpression plasmids based on transfecting miR-195 mimetics and miR-NC. Western blot results showed that *CYP4F11* overexpression significantly restored the suppression of CYP4F11 caused by miR-195 overexpression (Fig. 5G). The reductions in cell proliferation (Fig. 5H) and migration capacities (Fig. 5I) of A549/PC9 cells caused by overexpression of miR-195 were also significantly restored. Taken together, the results indicated that miR-195 inhibited tumor cell growth and migration by targeting *CYP4F11 in vitro*.

CYP4F11 is mainly localized in mitochondria

The subcellular organelle localization of proteins has important implications for exploring their specific biological functions. Therefore, we performed an immunofluorescence assay to determine the subcellular localization of CYP4F11 in A549 cells. We detected the following markers of each organelle: calnexin (endoplasmic reticulum), GM130 (Golgi apparatus), EEA1 (early endosome), CD63 (late endosome), LAMP1 (lysosome), and TOM20 (mitochondrial). The result showed that CYP4F11 was co-localized with TOM20 (Fig. 6A). Subsequently, we also selected three lung cancer patient tissues for tissue immunofluorescence, co-labeling CYP4F11 and TOM20, and the results were consistent with those observed in the cell-based experiments (Fig. 6B). Additionally, siRNA-mediated *CYP4F11* knockdown caused loss of mitochondrial DNA content as evidenced by reduced quantification of mitochondrial D-loop and Cytochrome b DNA content using qRT-PCR (*$P < 0.05$, Fig. 6C). The above results indicate that CYP4F11 is mainly localized in the

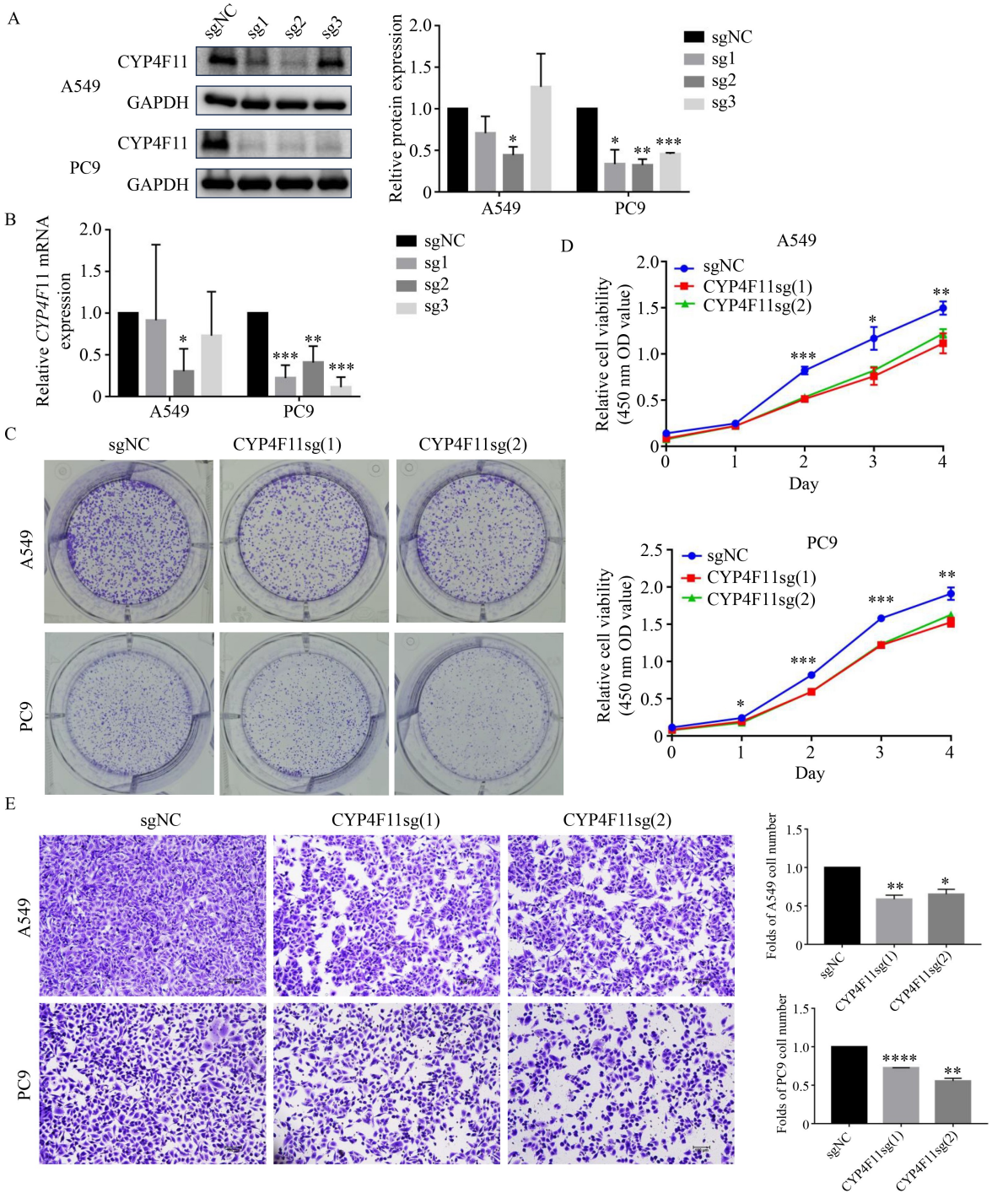

Fig. 3 Knockout of *CYP4F11* inhibits proliferation and migration in A549 and PC9 cells. (A) Western blot analysis of CYP4F11 protein expression in *CYP4F11*-knockout A549 and PC9 cells. (B) Compared with sg-NC group, the RNA levels of *CYP4F11* in A549 and PC9 cells treated with *CYP4F11*-sgRNA were significantly reduced, with fragment 2 (sg2) showing the most pronounced effect (**$P < 0.01$). (C) The colony formation assays indicated the reduced colony rate in A549 and PC9 cells treated with *CYP4F11*-sgRNA (1, 2). (D) The cell growth curve also showed the retard of A549 and PC9 cells treated with *CYP4F11*-sgRNA (1, 2) compared with NC. (E) The results of the Transwell assay (representative micrographs are presented) demonstrated the inhibition of migration in the *CYP4F11*-sgRNA (1, 2) group, and the relative migration rate was calculated.

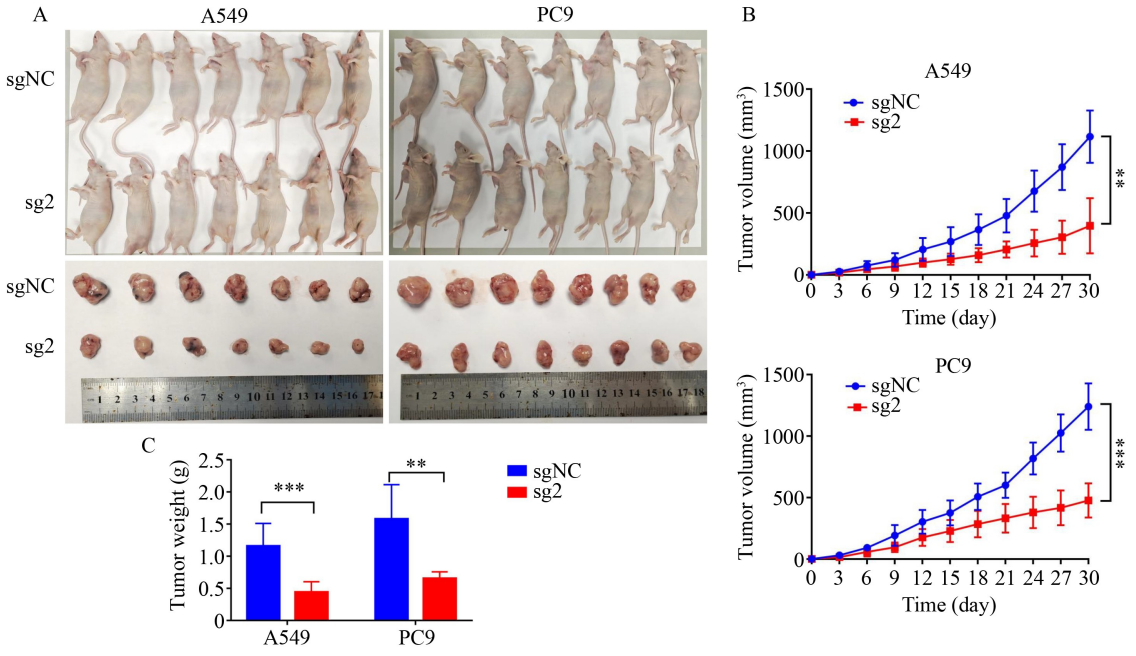

Fig. 4 sgRNA-mediated stable knockout of *CYP4F11* in A549 and PC9 cells reduces tumor growth in the mouse xenograft model. (A) Tumor xenografts were dissected from the sacrificed nude mice. (B) Tumor size was measured twice a week for up to 4 weeks. Tumor volume was calculated based on tumor width (W) and length (L) ($W^2 \times L/2$, with W < L). Data shown in the graph is the mean ± SEM for 7 tumors per group. Tumor volume in mice injected with *CYP4F11*-sgRNA (2) transduced A549 and PC9 were significantly less compared to that in mice injected with NC-sgRNA transduced A549 and PC9. (C) The tumor weights were measured and compared.

mitochondria of cells.

Knocking down *CYP4F11* can promote ubiquitin-mediated degradation of ME2 metabolic enzymes in mitochondria

To investigate the specific metabolic substrates of CYP4F11 in mitochondria, we selected si-NC A549, si-*CYP4F11* A549, and si-NC PC9, si-*CYP4F11* PC9 cell lines for metabolomic sequencing (both sets of data were strictly controlled). The results showed that knocking down *CYP4F11* significantly reduced the content of malic acid, and the difference was statistically significant (**P < 0.01, Fig. 7A). We also used a Malic Acid Colorimetric Assay Kit to detect the actual malic acid content in two groups, and the results confirmed the sequencing results (Fig. 7B). Then, we validated the expression of all malic enzymes (MEs) after knocking down *CYP4F11* through qRT-PCR and found that the decrease in *ME2* was most significant in A549 and PC9 cells (*P < 0.05, Fig. 7C). Western blot analysis also confirmed that knocking down *CYP4F11* can reduce the expression of ME2 in A549 and PC9 cells (Fig. 7D). To validate the interaction, we performed the reciprocal co-IP assays and indeed verified that CYP4F11 binds to ME2 in A549 and PC9 cancer cells (Fig. 7E). Immunofluorescence experiments also demonstrated the co-localization of CYP4F11 and ME2 (Fig. S2A). CYP4F11 is localized mitochondria and has a cofactor degradation function, while ME2 is a metabolic enzyme located in mitochondria (Fig. S2B). The co-localization of CYP4F11 and ME2 in mitochondria has also been experimentally demonstrated (Fig. S2C). The above results lead us to speculate whether CYP4F11 exerts a degradation function on ME2.

To verify this hypothesis, we explored multiple degradation pathways, among which only the ubiquitin-proteasome pathway played a role. We found that the protein level of ME2 dramatically declined upon *CYP4F11* knockdown, while this reduction was completely restored by treating the cells with the proteasome inhibitor MG132 (Fig. 7F). Additionally, knockdown of *CYP4F11* shortened the half-life of ME2 protein, as indicated by the cycloheximide-chase experiment (Fig. 7G). Consistent with these findings, we also showed that knockdown of *CYP4F11* drastically enhances ME2 ubiquitination (Fig. 7H). Therefore, these findings demonstrate that knockdown of *CYP4F11* prompts ubiquitination-mediated proteolytic degradation of ME2 in NSCLC to regulate the carcinogenic potential.

Knock down of *CYP4F11* reverses the NSCLC-promoting effects of ME2 overexpression

To further confirm the effect and biological functions of ME2 in NSCLC cells, ME2 expression was knocked

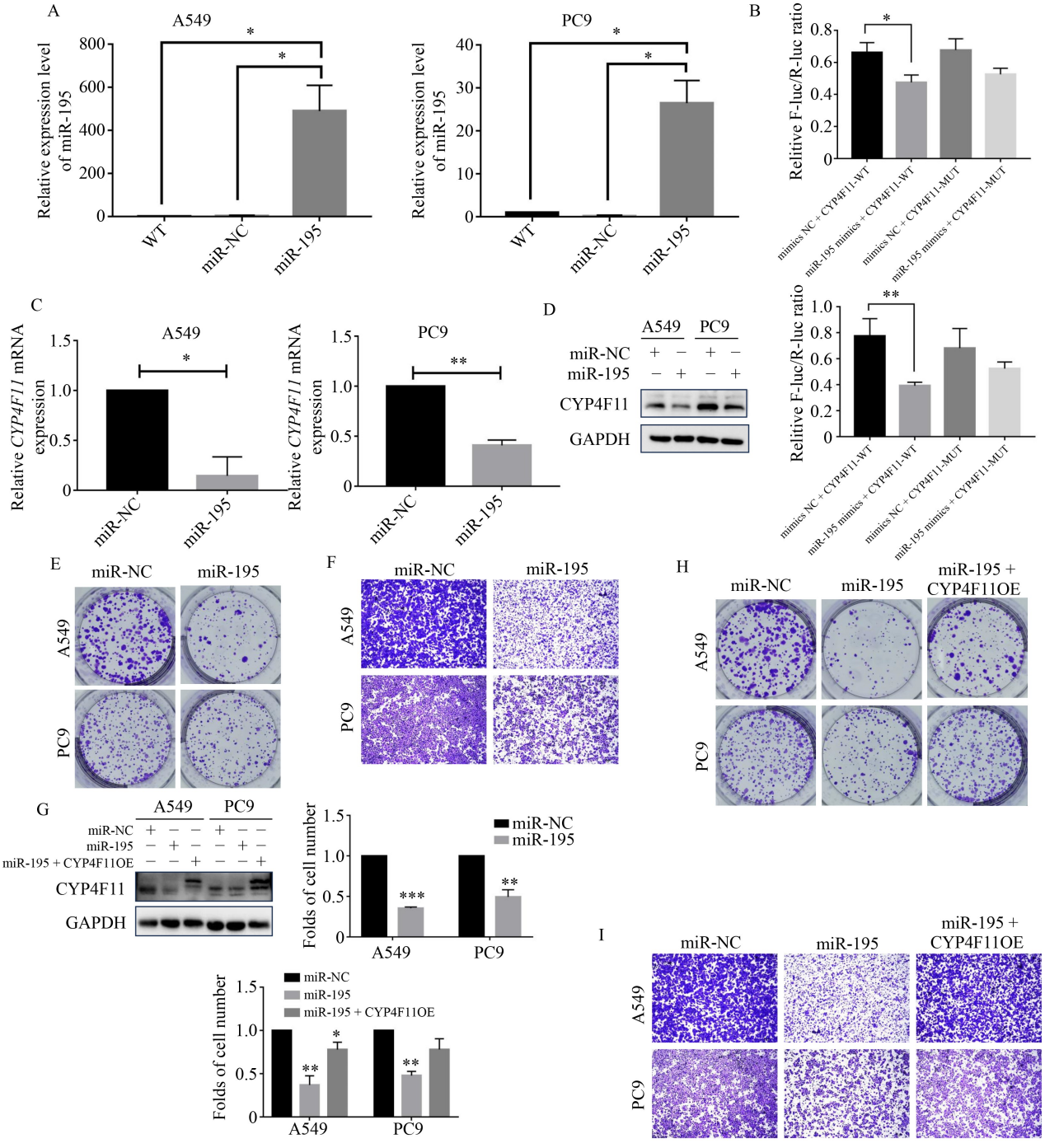

Fig. 5 Effects of the miR-195 overexpression on the inhibition of lung cancer cell proliferation *in vitro*. (A) miR-195 expression was detected in A549 and PC9 cells following miR-195 mimic or miR-NC transfection, and in untransfected (WT) cells using qRT-PCR. (B) The relative luciferase activity was determined in A549 and PC9 cells following co-transfection with a luciferase reporter plasmid (WT or MUT 3′-UTR *CYP4F11* cDNA), and miR-195 mimic or miR-NC. (C) mRNA and (D) protein levels of CYP4F11 in A549 and PC9 cells following transfection with miR-195 mimic or miR-NC were analyzed using qRT-PCR and Western blot analysis. GAPDH served as the internal control. (E) Colony formation was determined in A549 and PC9 cells transfected with miR-195 mimic or miR-NC. (F) Migration abilities of A549 and PC9 cells following transfection with miR-195 or miR-NC were detected by Transwell migration assays, respectively. (G) Protein levels of CYP4F11 in A549 and PC9 cells co-transfected with miR-195 mimic or miR-NC, and with or without *CYP4F11* cDNA were measured using reverse transcription-quantitative polymerase chain reaction and western blot analysis. (H) Cell proliferation and (I) Transwell migration assays were performed in A549/PC9 cells co-transfected with miR-195 mimic or miR-NC, and with or without *CYP4F11* cDNA. miR, microRNA; NC, negative control.

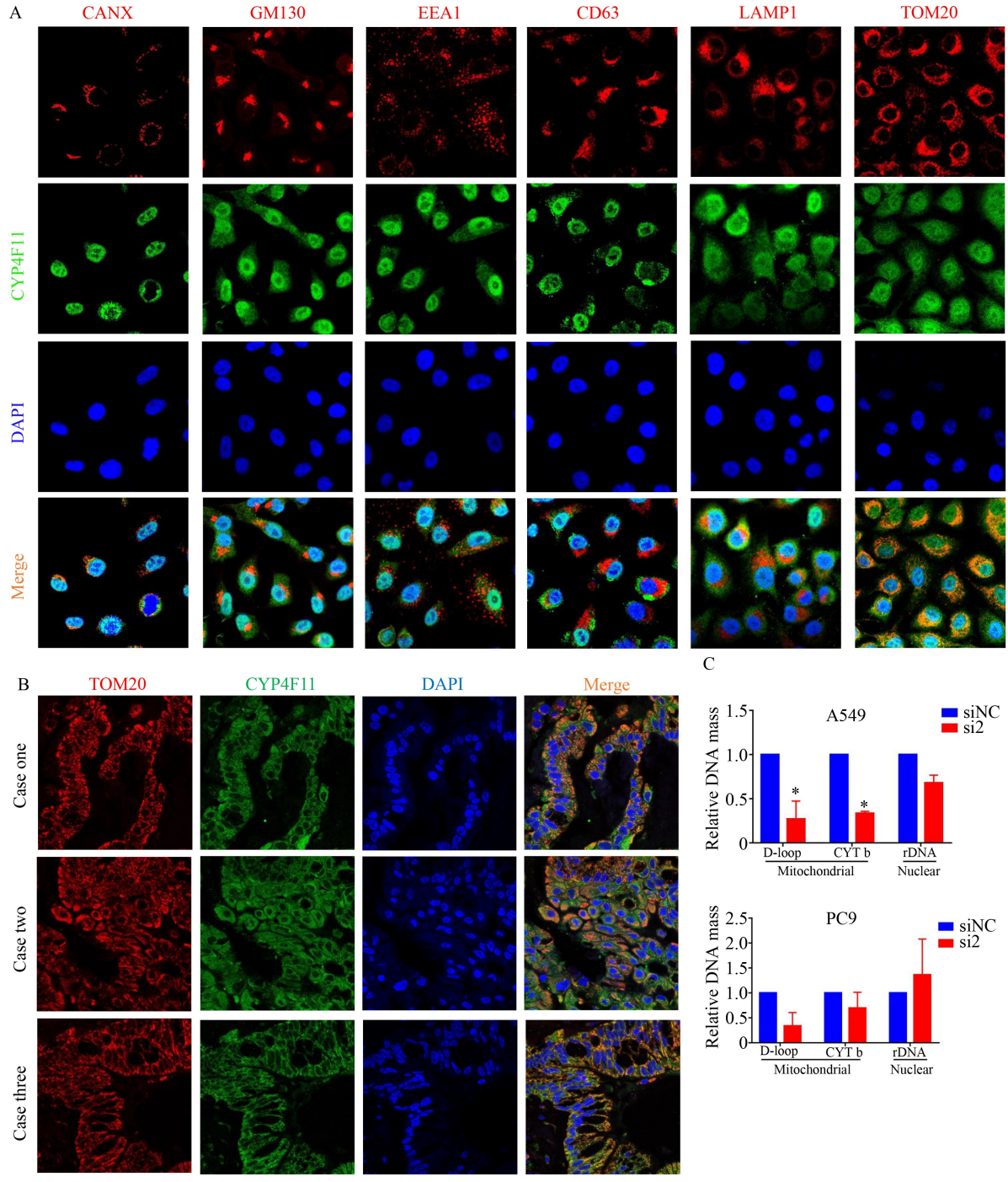

Fig. 6 (A) Stable cells indicated using anti-Calnexin, anti-GM130, anti-EEA1, anti-CD63, anti-Lamp1, and anti-TOM20 antibodies. (B) Tissue immunofluorescence in lung cancer tissue also showed co-localization of CYP4F11 and TOM20. (C) Transfection of *CYP4F11* siRNA reduced mitochondrial DNA content in A549 and PC9 cells. Total genomic DNA (mitochondrial and nuclear) was isolated 48 h after siRNA transfection and subjected to qRT-PCR using mitochondria-specific (D-loop and Cytochrome b) and nuclear (rDNA) DNA-specific primers.

down in A549 and PC9 cells using si-*ME2* and compared to the si-NC group. The data demonstrated that si-*ME2* significantly reduced the ME2 mRNA and protein expression levels in both A549 and PC9 cells, as target 3 demonstrating the most substantial effect and therefore selected for subsequent experiments (Fig. 8A and 8B). In addition, functional assays revealed that *ME2* knockdown significantly inhibited the tumor cell proliferation (Fig. 8C) and cell migration (Fig. 8D). Furthermore, to better verify that ME2 was a direct target of *CYP4F11*, the A549 and PC9 cells were simultaneously co-transfected with the *CYP4F11*-si2 or si-NC and *ME2*

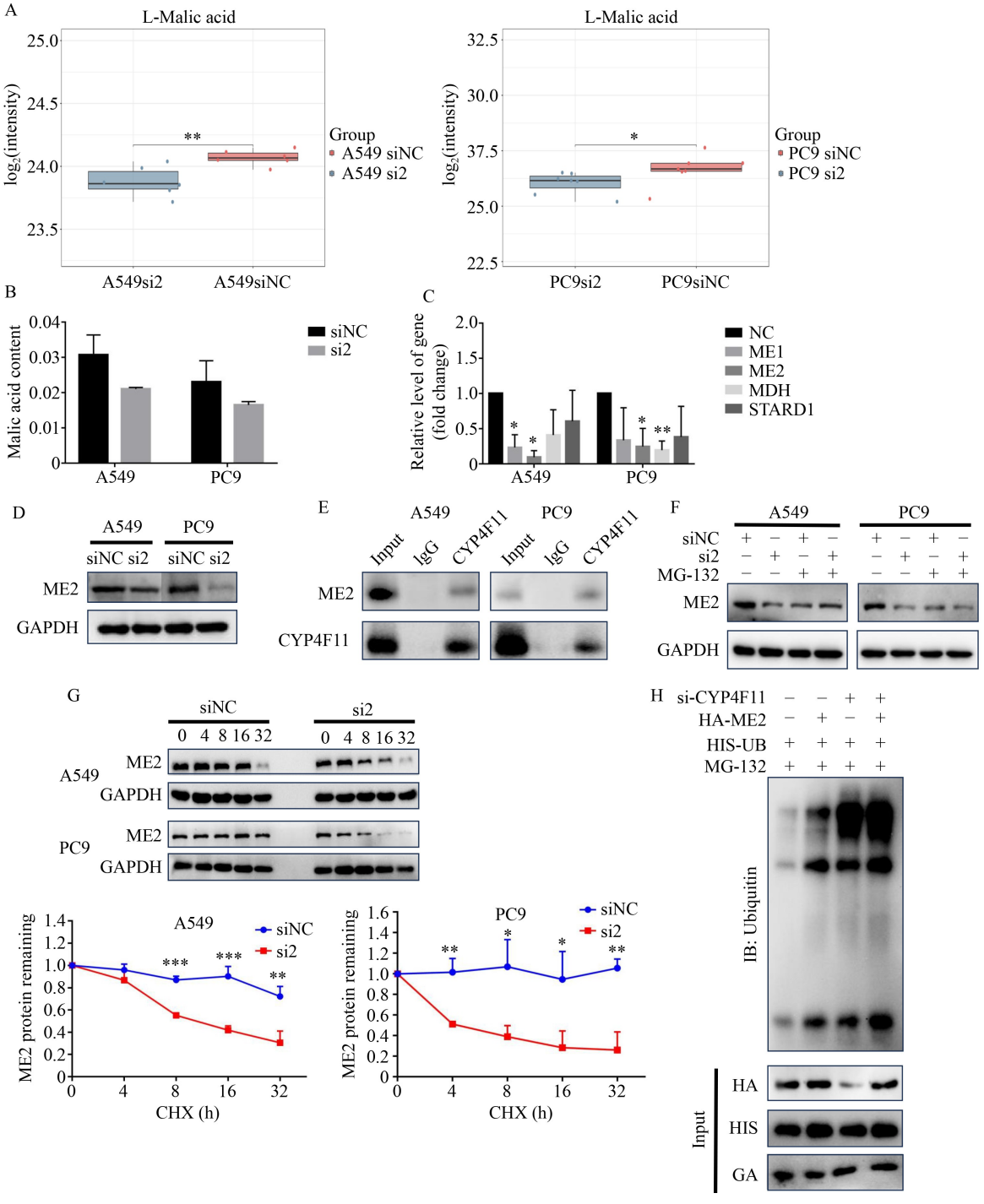

Fig. 7 CYP4F11 binds to and mediates the proteolytic degradation of ME2 in lung cancer. (A) Metabolomics results show that knocking out *CYP4F11* can significantly reduce malic acid content. (B) Biochemical assays also confirmed a decrease in malic acid content in mitochondria after knocking down *CYP4F11*. (C) The changes in the content of four malic enzymes after knocking down *CYP4F11* were explored using qRT-PCR experiments, and it was found that *ME2* had the most significant reduction effect (*$P < 0.05$). (D) Western blot results showed that knocking out *CYP4F11* can reduce the expression of ME2. (E) CYP4F11 interacts with ME2 by the reciprocal co-IP assays in A549 and PC9 cancer cells. (F) Knocking down *CYP4F11* in A549 and PC9 cells led to a decrease in ME2 protein levels, which was blocked by the proteasome inhibitor MG132 (10 μmol/L). (G) The half-life of ME2 was shortened upon *CYP4F11* low expression. The cells were treated with 0.2 mg/mL of cycloheximide (CHX) and harvested at different time points as indicated. The quantification of ME2 expression is shown in the lower panel. (H) The ubiquitination of ME2 was mediated by *CYP4F11*. Cells were transfected with combinations of plasmids encoding si-*CYP4F11*, HA-ME2, or His-Ub as indicated and treated with MG132 (10 μmol/L) for 6 h before being harvested for the IP assays using the anti-ubiquitin antibody. Results were presented as mean ± SD of three independent experiments.

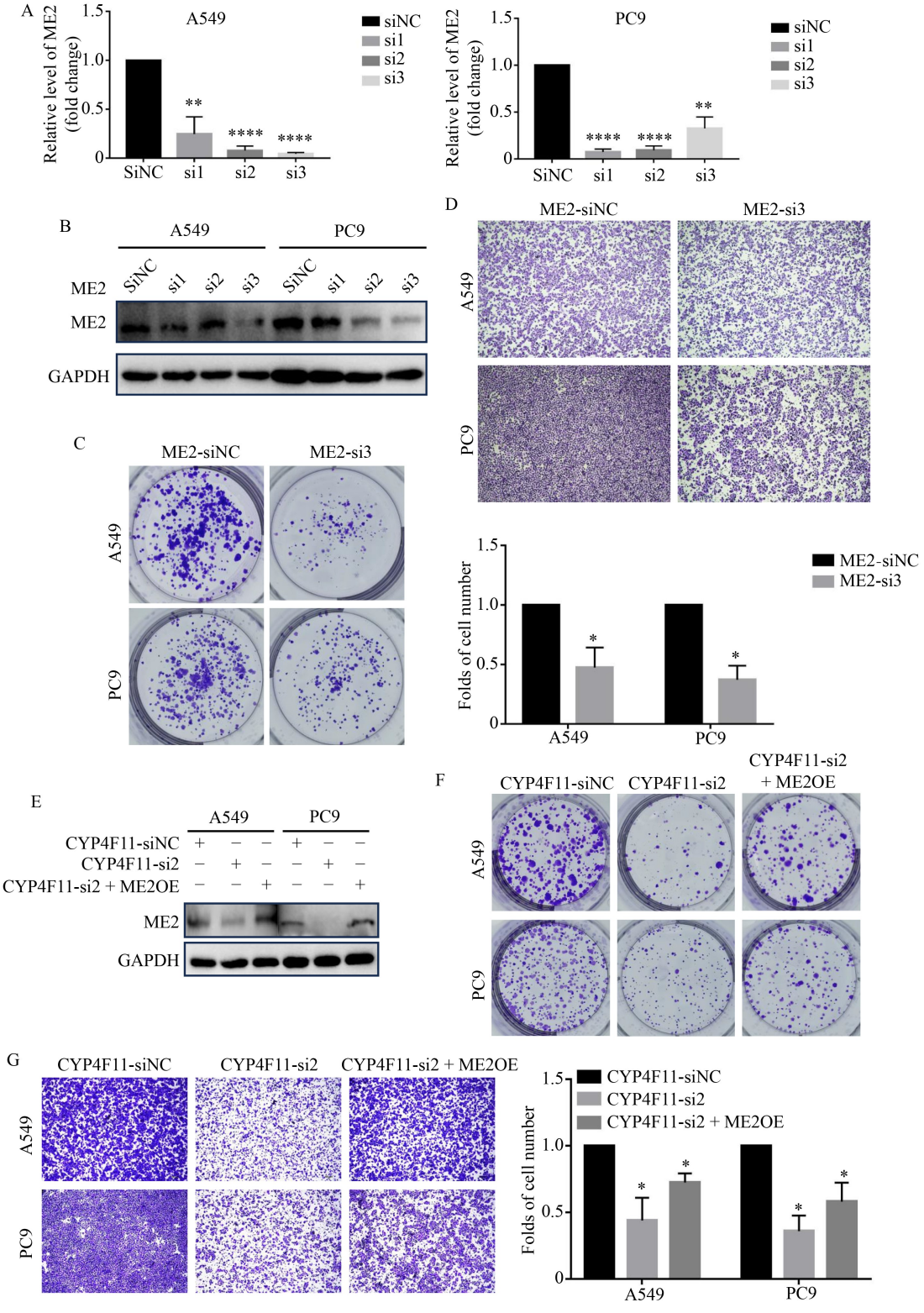

Fig. 8 Knockdown of *CYP4F11* reverses the pro-proliferative and migratory effects induced by ME2 overexpression (A) mRNA and (B) protein levels of ME2 in A549 and PC9 cells following transfection with si-*ME2* or si-NC were measured using qRT-PCR and Western blot analysis, respectively. GAPDH was used as internal controls, respectively. (C) Colony formation and (D) Transwell tumor cell migration assay in lung cancer cells transfected with si-*ME2* or si-NC. (E) Protein levels of ME2 in A549 and PC9 cells co-transfected with si-*CYP4F11* or si-NC, and with or without *ME2* cDNA were measured using Western blot analysis. (F) Colony formation and (G) Transwell tumor cell migration in A549 and PC9 cells co-transfected with si-*CYP4F11* or si-NC, and with or without ME2 cDNA. *$P < 0.05$ and **$P < 0.01$. NC, negative control; ME2, malic enzyme 2; si, siRNA.

overexpression plasmid. We found that ME2 overexpression using *ME2* cDNA transfection in *CYP4F11*-si2-expressing A549 and PC9 cells was able to partially reverse *CYP4F11* low expression-induced reduction of ME2 expression in A549 and PC9 cells (Fig. 8E). The ME2 overexpression also functionally rescued the suppressive effects of *CYP4F11* knockdown on tumor cell proliferation and migration (Fig. 8F and 8G). Taken together, the results indicated that *CYP4F11* promoted tumor cell proliferation and migration by targeting ME2 *in vitro*.

Discussion

The CYP4F enzyme is responsible for the metabolism of eicosane compounds [17]. CYP4F11 is an isomer of the 4F family that exhibits catalytic activity against endogenous eicosadiene (leukotriene B4), arachidonic acid, prostaglandins and lipoxygenase products, hydroxy eicosatetraenoic acid, and commonly used drugs (erythromycin, amphetamine, and chlorpromazine) [14,18]. CYP4F11 is believed to be primarily involved in the metabolism of fatty acids (3-hydroxy palmitate) and arachidonic acid metabolites [19]. At present, a series of reports have shown that multiple compounds and pathways are involved in the regulation of *CYP4F11* expression, such as activated B cell light chain enhancer nuclear factor B (NF-κB) can inhibit the expression of *CYP4F11* in human liver cancer cell line (HepG2) [20]. In HaCaT keratinocytes, the *CYP4F11* gene is positively regulated by various signaling pathways such as RXR and JNK [21]. This study indicates that *CYP4F11* has potential value in tumor development. However, the molecular mechanisms of *CYP4F11* that lead to the progression of tumors remain unclear, especially since the CYP4F11 superfamily has an individual role in different types of cancer, and its role in lung cancer is rarely studied. Herein, our clinical data, based on TCGA and GEO data sets, IHC, and prognosis analysis, reveals that CYP4F11 is a prognostic biomarker that is upregulated in lung cancer. The functional impact and mechanism of the dysregulation of CYP4F11 in lung cancer remains to be determined.

To explore the role and potential mechanisms of *CYP4F11* in lung cancer, our research group conducted a series of cellular and animal experiments from various aspects using *in vitro*, *in vivo*, and *ex vivo* approaches. We conducted an immunohistochemical assay on the cancerous tissue and its corresponding adjacent tissues of 235 NSCLC patients. The results showed that the expression of *CYP4F11* in the cancerous tissue of lung cancer patients was significantly higher than that in adjacent tissues, and the high expression of *CYP4F11* predicted poor prognosis. Through extensive cytological experiments, we have confirmed that knocking down *CYP4F11* significantly weakened the proliferation and migration ability of NSCLC cells, suggesting that *CYP4F11* may be involved in the carcinogenesis and development of NSCLC.

Through the TargetScan database and dual luciferase reporter assay, we identified *CYP4F11* as a downstream target of miR-195, and the expression level of *CYP4F11* could be regulated by miR-195. The hsa-miR-195 gene is located on chromosome 17p13.1 from 6 881 953 bp to 6 862 065 bp [22]. Previous studies have shown that miR-195 might act as a tumor suppressor in several types of cancers. For example, it was reported that miR-195-5p suppressed the proliferation, migration, and invasion ability of oral squamous cell carcinoma by targeting *TRIM14* [23]. It was shown that miR-195 expression was downregulated in lung cancer samples compared with normal tissues. Furthermore, miR-195 suppressed lung cancer growth and metastasis [24]. In the present research, *CYP4F11* was identified as the target of miR-195. First, miR-195 repressed *CYP4F11* expression by binding to the 3′-UTR of *CYP4F11*, which was identified by the luciferase reporter assay. In addition, the expression of *CYP4F11* in lung cancer cell lines was remarkably decreased by miR-195 transfection. More importantly, *CYP4F11* restoration abolished the suppressed effects caused by miR-195 overexpression. These results suggested that *CYP4F11* acted as an oncogenic role in the development of NSCLC and miR-195 repressed NSCLC cell growth by targeting *CYP4F11*.

The subsequent immunofluorescence experiments showed that CYP4F11 was mainly localized in mitochondria. As is well known, mitochondria are organelles involved in biosynthesis, bioenergy, and signal transduction, which are crucial for physiologic adaptation and cellular stress responses to the environment [25]. Mitochondria play an important role in the carcinogenesis and development of lung cancer. This project has identified a powerful gene — *CYP4F11* that affects the progression of NSCLC. And revealed that *CYP4F11* affects lung cancer progression by regulating the concentration of malic acid in mitochondria.

Participating in cofactor degradation is also one of the important functions of CYP4F11 [15]. The results of metabolomics and cellular experiments both indicate that knocking down *CYP4F11* can lead to a decrease in malic acid in cell mitochondria and affect the metabolic status of NSCLC cells, thereby affecting their progression. Notably, MEs catalyze the oxidative decarboxylation of malate to generate pyruvate and either NADPH or NADH with NAD(P) functioning as a coenzyme. In mammalian cells, there are three isoforms of MEs, including cytosolic NADP-dependent isoform (ME1), mitochondrial NAD(P)-dependent isoform (ME2), and mitochondrial NAD-dependent isoform (ME3). Compared with *ME3*, *ME2* is higher in cells, and ME2 plays a more important

regulatory role in cell metabolism. ME2 regulates TCA flux in response to cellular demands for energy, carbon skeletons, and reducing equivalents [26]. In addition, ME2 significantly enhances glutamine and lipid metabolism in cancer cells, in response to their high metabolic demand [27]. Aberrant *ME2* expression has been found in a variety of cancers, and 2-hydroxyglutarate (2-HG) generated by ME2 is involved in the stabilization of mutant p53 [28,29], while α-ketoglutarate (α-KG) produced by ME2 promotes cell cycle progression by upregulating the transcription of cyclin D1 [30]. However, little is known about the mechanism regulating the activity of ME2. In this study, we have demonstrated that knocking down *CYP4F11* promotes the degradation of ME2 metabolic enzymes in mitochondria, which is mediated by the ubiquitin-proteasome pathway. However, further exploration is needed to determine the specific mitochondrial functional changes caused by CYP4F11 through ME2.

There are three main pathways for protein degradation in eukaryotic cells: (1) lysosomal pathway, (2) ubiquitination pathway, and (3) caspase pathway [31]. The ubiquitin-proteasome system (UPS) represents the major route by which the cell degrades unwanted proteins [32]. In the canonical mode of protein degradation, the conjugation of ubiquitin to substrates serves as the signal for proteasomal targeting and subsequent degradation [33,34]. Ubiquitination occurs through a cascade of three enzymes: specifically, ubiquitin was activated by the E1 enzyme, then transferred to an E2 ubiquitin-conjugating enzyme, and finally to the target substrate by an E3 ligase [35]. E3 ligases play the most crucial role in providing specificity [36] by interacting with their substrates through the direct recognition of short peptide motifs termed degrons. Degrons are defined as the minimal element that is sufficient for recognition and degradation by the proteolytic pieces of machinery, and an important property of degrons is that they are transferable [37]. *CYP4F11* and *ME2*, as oncogenes, play important roles in promoting the progression of lung cancer. The experimental results in this study indicate that knocking down *CYP4F11* promotes ME2 ubiquitination degradation and inhibit tumor progression, providing us with a new approach.

Our findings reveal that while *CYP4F11* does not directly modulate glycolytic enzymes, its mitochondrial localization enables profound metabolic reprogramming through ME2 degradation. ME2 serves as a crucial metabolic nexus between mitochondrial function and glycolytic flux through multiple interconnected mechanisms [38]. First, by catalyzing malate decarboxylation, ME2 generates pyruvate for lactate production —the terminal glycolytic product —while simultaneously producing NAD(P)H to maintain redox balance essential for glycolytic enzyme activity (e.g., GAPDH) [39]. Second, ME2 sustains TCA cycle anaplerosis by regulating mitochondrial pyruvate pools and PDH activity, thereby indirectly modulating glycolytic flux through citrate-mediated allosteric inhibition of PFK1 [40]. Third, ME2-derived NADPH plays dual roles in both counteracting glycolysis-associated ROS through GSH regeneration and diverting glucose flux into the pentose phosphate pathway (PPP) pathway [41,42]. In tumors, ME2's glycolytic regulation becomes particularly significant. We observed that ME2 deficiency leads to α-KG reduction, resulting in PHD2 inhibition and subsequent HIF-1α stabilization [43]. This transcriptional reprogramming upregulates key glycolytic enzymes including HK2 and PFKFB3. Furthermore, ME2-generated pyruvate directly feeds LDHA-mediated lactate production, thereby sustaining the characteristic Warburg effect of cancer metabolism [44]. These findings position the *CYP4F11*-*ME2* axis as a novel regulator of cancer cell metabolism through its bidirectional control of glycolysis —both supplying essential substrates and modulating enzymatic activity via redox/epigenetic mechanisms [45,46]. The therapeutic implications of this pathway are substantial, as tumors appear to critically depend on this metabolic flexibility. Future studies will focus on: (1) characterizing the precise E3 ligase involved in *CYP4F11*-mediated ME2 ubiquitination, (2) experimental validation of *CYP4F11*-mediated metabolic pathway regulation through ME2 degradation, and (3) developing small molecule inhibitors targeting this axis. These investigations will further validate the clinical potential of metabolic intervention in NSCLC treatment.

Conclusions

Overall, our study revealed that the *CYP4F11*/miR-195/*ME2* axis plays a vital role in regulating cancer progression. miR-195 plays an important role in regulating *CYP4F11* transcription. Inhibiting *CYP4F11* expression promotes the ubiquitin-mediated degradation of the mitochondrial metabolic enzyme ME2, which may represent a promising therapeutic strategy for lung cancer and warrants further investigation. Further investigation of the expression profile and clinicopathological significance of the *CYP4F11*/miR-195/*ME2* axis is warranted.

Acknowledgements

This study was supported by the National Natural Science Foundation of China (Nos. 82060529 and 82172748) and the Guangdong Basic and Applied Basic Research Foundation (No. 2023A1515110567).

Compliance with ethics guidelines

Conflicts of interest Shan Shi, Jiao Zhou, Qiuyun Luo, Hongtao Chen, Jing Yang, Liqiong Yang, Lin Zhang, Hongyu Zhang, and Dajun Yang declare that they have no conflict of interest.

The *in vivo* animal experiments were approved by animal experimentation ethics and carried out under the guidance of the Sun Yat-Sen University Committee for Use and Care of Laboratory Animals (Approval number: 2022001130). All institutional and national guidelines for the care and use of laboratory animals were followed. The tissue sections of these patients were obtained from the Department of Pathology of the fifth affiliated hospital of Sun Yat-sen University. This study acquired the approval of the Ethics Committee of the fifth affiliated hospital of Sun Yat-sen University before specimen collection. Written informed consent was obtained from all the patients before surgery. Additional informed consent was obtained from all patients for which identifying information is included in this article.

Electronic supplementary material Supplementary material is available in the online version of this article at https://doi.org/10.1007/s11684-025-1166-y and is accessible to authorized users.

References

1. Xia C, Dong X, Li H, Cao M, Sun D, He S, Yang F, Yan X, Zhang S, Li N, Chen W. Cancer statistics in China and United States, 2022: profiles, trends, and determinants. Chin Med J (Engl) 2022; 135(5): 584–590
2. Li J, Kwok HF. Current strategies for treating NSCLC: from biological mechanisms to clinical treatment. Cancers (Basel) 2020; 12(6): 1587
3. Xu J, Tian L, Qi W, Lv Q, Wang T. Advancements in NSCLC: from pathophysiological insights to targeted Treatments. Am J Clin Oncol 2024; 47(6): 291–303
4. Elfaki I, Mir R, Almutairi FM, Duhier FMA. Cytochrome P450: polymorphisms and roles in cancer, diabetes and atherosclerosis. Asian Pac J Cancer Prev 2018; 19(8): 2057–2070
5. Hashizume T, Imaoka S, Hiroi T, Terauchi Y, Fujii T, Miyazaki H, Kamataki T, Funae Y. cDNA cloning and expression of a novel cytochrome p450 (cyp4f12) from human small intestine. Biochem Biophys Res Commun 2001; 280(4): 1135–1141
6. Bylund J, Bylund M, Oliw EH. cDna cloning and expression of CYP4F12, a novel human cytochrome P450. Biochem Biophys Res Commun 2001; 280(3): 892–897
7. Kalsotra A, Cui X, Anakk S, Hinojos CA, Doris PA, Strobel HW. Renal localization, expression, and developmental regulation of P450 4F cytochromes in three substrains of spontaneously hypertensive rats. Biochem Biophys Res Commun 2005; 338(1): 423–431
8. Christmas P, Carlesso N, Shang H, Cheng SM, Weber BM, Preffer FI, Scadden DT, Soberman RJ. Myeloid expression of cytochrome P450 4F3 is determined by a lineage-specific alternative promoter. J Biol Chem 2003; 278(27): 25133–25142
9. Bylund J, Hidestrand M, Ingelman-Sundberg M, Oliw EH. Identification of CYP4F8 in human seminal vesicles as a prominent 19-hydroxylase of prostaglandin endoperoxides. J Biol Chem 2000; 275(29): 21844–21849
10. Cui X, Strobel HW. Cloning and characterization of the rat cytochrome P450 4F5 (CYP4F5) gene. Gene 2002; 297(1–2): 179–187
11. Zhang JE, Klein K, Jorgensen AL, Francis B, Alfirevic A, Bourgeois S, Deloukas P, Zanger UM, Pirmohamed M. Effect of genetic variability in the CYP4F2, CYP4F11, and CYP4F12 genes on liver mRNA levels and warfarin response. Front Pharmacol 2017; 8: 323
12. Cui X, Nelson DR, Strobel HW. A novel human cytochrome P450 4F isoform (CYP4F11): cDNA cloning, expression, and genomic structural characterization. Genomics 2000; 68(2): 161–166
13. Goldstein I, Rivlin N, Shoshana OY, Ezra O, Madar S, Goldfinger N, Rotter V. Chemotherapeutic agents induce the expression and activity of their clearing enzyme CYP3A4 by activating p53. Carcinogenesis 2013; 34(1): 190–198
14. Kalsotra A, Turman CM, Kikuta Y, Strobel HW. Expression and characterization of human cytochrome P450 4F11: putative role in the metabolism of therapeutic drugs and eicosanoids. Toxicol Appl Pharmacol 2004; 199(3): 295–304
15. Winterton SE, Capota E, Wang X, Chen H, Mallipeddi PL, Williams NS, Posner BA, Nijhawan D, Ready JM. Discovery of cytochrome P450 4F11 activated inhibitors of stearoyl coenzyme a desaturase. J Med Chem 2018; 61(12): 5199–5221
16. Theodoropoulos PC, Gonzales SS, Winterton SE, Rodriguez-Navas C, McKnight JS, Morlock LK, Hanson JM, Cross B, Owen AE, Duan Y, Moreno JR, Lemoff A, Mirzaei H, Posner BA, Williams NS, Ready JM, Nijhawan D. Discovery of tumor-specific irreversible inhibitors of stearoyl CoA desaturase. Nat Chem Biol 2016; 12(4): 218–225
17. Hsu MH, Savas U, Griffin KJ, Johnson EF. Human cytochrome p450 family 4 enzymes: function, genetic variation and regulation. Drug Metab Rev 2007; 39(2–3): 515–538
18. Choudhary MI, Nawaz SA, ul-Haq Z, Lodhi MA, Ghayur MN, Jalil S, Riaz N, Yousuf S, Malik A, Gilani AH, ur-Rahman A. Withanolides, a new class of natural cholinesterase inhibitors with calcium antagonistic properties. Biochem Biophys Res Commun 2005; 334(1): 276–287
19. Yi M, Cho SA, Min J, Kim DH, Shin JG, Lee SJ. Functional characterization of a common CYP4F11 genetic variant and identification of functionally defective CYP4F11 variants in erythromycin metabolism and 20-HETE synthesis. Arch Biochem Biophys 2017; 620: 43–51
20. Zhang T, Zhan Z, Chen Y, Chen J, Han W, Liang Z, Liu Q, Liu S, Tang L. Regulation of cytochrome P450 4F11 expression by liver X receptor alpha. Int Immunopharmacol 2021; 90: 107240
21. Wang Y, Bell JC, Keeney DS, Strobel HW. Gene regulation of CYP4F11 in human keratinocyte HaCaT cells. Drug Metab Dispos 2010; 38(1): 100–107
22. Liu J, Ren L, Li S, Li W, Zheng X, Yang Y, Fu W, Yi J, Wang J, Du G. The biology, function, and applications of exosomes in cancer. Acta Pharm Sin B 2021; 11(9): 2783–2797
23. Wang T, Ren Y, Liu R, Ma J, Shi Y, Zhang L, Bu R. miR-195–5p suppresses the proliferation, migration, and invasion of oral squamous cell carcinoma by targeting TRIM14. BioMed Res Int 2017; 2017: 7378148

24. Long Z, Wang Y. miR-195–5p suppresses lung cancer cell proliferation, migration, and invasion via FOXK1. Technol Cancer Res Treat 2020; 19: 1533033820922587
25. Nunnari J, Suomalainen A. Mitochondria: in sickness and in health. Cell 2012; 148(6): 1145–1159
26. Jiang P, Du W, Mancuso A, Wellen KE, Yang X. Reciprocal regulation of p53 and malic enzymes modulates metabolism and senescence. Nature 2013; 493(7434): 689–693
27. Wang YP, Sharda A, Xu SN, van Gastel N, Man CH, Choi U, Leong WZ, Li X, Scadden DT. Malic enzyme 2 connects the Krebs cycle intermediate fumarate to mitochondrial biogenesis. Cell Metab 2021; 33(5): 1027–41.e8
28. Zhao M, Yao P, Mao Y, Wu J, Wang W, Geng C, Cheng J, Du W, Jiang P. Malic enzyme 2 maintains protein stability of mutant p53 through 2-hydroxyglutarate. Nat Metab 2022; 4(2): 225–238
29. Dey P, Baddour J, Muller F, Wu CC, Wang H, Liao WT, Lan Z, Chen A, Gutschner T, Kang Y, Fleming J, Satani N, Zhao D, Achreja A, Yang L, Lee J, Chang E, Genovese G, Viale A, Ying H, Draetta G, Maitra A, Wang YA, Nagrath D, DePinho RA. Genomic deletion of malic enzyme 2 confers collateral lethality in pancreatic cancer. Nature 2017; 542(7639): 119–123
30. Yang Y, Zhang Z, Li W, Si Y, Li L, Du W. αKG-driven RNA polymerase II transcription of cyclin D1 licenses malic enzyme 2 to promote cell-cycle progression. Cell Rep 2023; 42(7): 112770
31. Hanzl A, Winter GE. Targeted protein degradation: current and future challenges. Curr Opin Chem Biol 2020; 56: 35–41
32. Kwon YT, Ciechanover A. The ubiquitin code in the ubiquitin-proteasome system and autophagy. Trends Biochem Sci 2017; 42(11): 873–886
33. Sommer T, Wolf DH. The ubiquitin-proteasome-system. Biochim Biophys Acta Mol Cell Res 2014; 1843(1): 1
34. Paudel RR, Lu D, Roy Chowdhury S, Monroy EY, Wang J. Targeted protein degradation via lysosomes. Biochemistry 2023; 62(3): 564–579
35. Pickart CM. Mechanisms underlying ubiquitination. Annu Rev Biochem 2001; 70(1): 503–533
36. Zheng N, Shabek N. Ubiquitin ligases: structure, function, and regulation. Annu Rev Biochem 2017; 86(1): 129–157
37. Lucas X, Ciulli A. Recognition of substrate degrons by E3 ubiquitin ligases and modulation by small-molecule mimicry strategies. Curr Opin Struct Biol 2017; 44: 101–110
38. Ding XB, Wang XX, Xia DH, Liu H, Tian HY, Fu Y, Chen YK, Qin C, Wang JQ, Xiang Z, Zhang ZX, Cao QC, Wang W, Li JY, Wu E, Tang BS, Ma MM, Teng JF, Wang XJ. Impaired meningeal lymphatic drainage in patients with idiopathic Parkinson's disease. Nat Med 2021; 27(3): 411–418
39. Sternson SM, Atasoy D, Betley JN, Henry FE, Xu S. An emerging technology framework for the neurobiology of appetite. Cell Metab 2016; 23(2): 234–253
40. Okun E, Dikshtein Y, Carmely A, Saida H, Frei G, Sela BA, Varshavsky L, Ofir A, Levy E, Albeck M, Sredni B. The organotellurium compound ammonium trichloro (dioxoethylene-o, o′) tellurate reacts with homocysteine to form homocystine and decreases homocysteine levels in hyperhomocysteinemic mice. FEBS J 2007; 274(12): 3159–3170
41. Cabral H, Matsumoto Y, Mizuno K, Chen Q, Murakami M, Kimura M, Terada Y, Kano MR, Miyazono K, Uesaka M, Nishiyama N, Kataoka K. Accumulation of sub-100 nm polymeric micelles in poorly permeable tumours depends on size. Nat Nanotechnol 2011; 6(12): 815–823
42. Hildebrand D, Bode KA, Rieß D, Cerny D, Waldhuber A, Römmler F, Strack J, Korten S, Orth JHC, Miethke T, Heeg K, Kubatzky KF. Granzyme A produces bioactive IL-1β through a nonapoptotic inflammasome-independent pathway. Cell Rep 2014; 9(3): 910–917
43. Tang F, Quan Y, Xin ZT, Wrammert J, Ma MJ, Lv H, Wang TB, Yang H, Richardus JH, Liu W, Cao WC. Lack of peripheral memory B cell responses in recovered patients with severe acute respiratory syndrome: a six-year follow-up study. J Immunol 2011; 186(12): 7264–7268
44. Wang P, González MC, Hidalgo CA, Barabási AL. Understanding the spreading patterns of mobile phone viruses. Science 2009; 324(5930): 1071–1076
45. Xu J, Wang Q. Ejaculate economics: an experimental test in a moth. Biol Lett 2014; 10(1): 20131031
46. Losman JA, Looper RE, Koivunen P, Lee S, Schneider RK, McMahon C, Cowley GS, Root DE, Ebert BL, Kaelin WG Jr. (R)-2-hydroxyglutarate is sufficient to promote leukemogenesis and its effects are reversible. Science 2013; 339(6127): 1621–1625